Computer simulation of Au(001)/Ni multilayers: comparison with experiments

1995 J. Phys.: Condens. Matter 7 6407

(http://iopscience.iop.org/0953-8984/7/32/007)

J. Phys.: Condens. Matter 7 (1995) 6407–6421. Printed in the UK

Computer simulation of Au(001)/Ni multilayers: comparison with experiments

Thierry Deutsch, Pascale Bayle, Frédéric Lançon and Jany Thibault

CEA/Département de Recherche Fondamentale sur la Matière Condensée, SP2M, CENG, 17 rue des Martyrs, 38054 Grenoble Cédex 9, France

Received 24 April 1995

Abstract. The structure of thin Ni film on Au(001) and Au(001)/Ni multilayers is studied as a function of the thickness of Ni using a semiempirical potential based on the tight-binding second-moment approximation. It is shown that the stable structure is pseudomorphic for a thickness less than five monolayers and $[2\bar{1}\bar{1}0]$ hcp or 4H for a greater thickness with close-packed planes perpendicular to the interfaces. Moreover, we show that a thin Ni film grown on Au(001) substrate is covered by at least one monolayer of Au. We compare our results with high-resolution electronic microscopy (HREM) and x-ray diffraction.

1. Introduction

Metallic multilayered films with artificial superstructures are fabricated by alternately depositing layers such that a one-dimensional composition modulation is produced. There is a strong interest in modifying physical properties of these materials by controlling growth parameters on an atomic level with molecular beam epitaxy (MBE). The basis for any understanding of multilayer properties must lie in the structure of thin adsorbate film. Several systems like Au/Ni [1–5], Au/Co [6–9] and Ag/Ni [10–12] have been extensively investigated in recent years with different growth directions.

The Au/Ni system is considered as a model system and has the following features

(i) Both Au and Ni metals have fcc structures.

(ii) In spite of a large difference in lattice constants ($a_{Au} = 0.4079$ nm, $a_{Ni} = 0.3524$ nm and $(a_{Ni} - a_{Au})/a_{Au} = -0.14$), epitaxial growth of Ni films on [001]-oriented Au films is coherent if the thickness of the Ni film is less than a critical value.

(iii) The phase diagram of the bulk Au–Ni alloy shows a simple miscibility gap with a critical temperature at 810 °C. Mutual solubilities of Au and Ni are very limited at lower temperatures.

Experimentally, *in situ* RHEED (reflection high energy electron diffraction) and x-ray diffraction measurements indicate that Ni grows epitaxially in (100) Au/Ni multilayers [13] and during the growth process two forms of growth have been formed: for less than five monolayers deposited, a pseudomorphic Ni grew (Ni and Au have the same in-plane lattice) and for five or more monolayers, fcc Ni(011) with many twins and stacking faults was present.

In this article, we investigate numerically the structure of the Au/Ni oriented [001] multilayers at 0 K and compare them with experimental results. We used a semi empirical

0953-8984/95/326407+15$19.50

potential [14–16] based on the tight-binding second-moment approximation of the tight-binding description of metallic cohesion. This potential has been widely used for different studies on structural properties [14, 17], noble metals [18], surface relaxation [19–21] and solid solutions like AuNi [3] and NiAl [22].

The article is organized as follows: after a brief review of the static properties of the employed interatomic potential, the phonon dispersion curves and miscellaneous finite-temperature properties are presented. Then, the structure of Au/Ni multilayers with abrupt interfaces as a function of the Ni layer thickness is discussed. We have considered the case of a large Au layer thickness as compared to Ni. With a thickness less than five monolayers, a pseudomorphic Ni has the lowest formation energy and it transforms for a greater thickness into a hexagonal phase (hcp or 4H) with close-packed planes perpendicular to the interfaces. Since a structural transformation of the Ni film deposited has been observed by RHEED during the growth [13], we also study a Ni film on a Au(001) buffer. We show that a Au monolayer on the top of the Ni film lowers the formation energy of the system. To explain the presence of Au atoms on the top layer, we suggest an exchange mechanism between a Ni atom and a Au atom on the surface. Such an exchange mechanism has been observed by molecular dynamics.

We compare our results with those obtained by HREM [23] and by x-ray diffraction [24]. A partial presentation of the results has been already made in [25].

2. Interatomic potential

2.1. Generality

We recall briefly the characteristic of the potential described at length by Eymery *et al* [3].

The energy of a monatomic metal can be approximated by

$$E = \frac{1}{N}\sum_{i}^{N}\left[\sum_{j} A\exp\left\{-p\left(\frac{r_{ij}}{r_0}-1\right)\right\} - \left(\sum_{j}\xi^2\exp\left\{-2q\left(\frac{r_{ij}}{r_0}-1\right)\right\}\right)^{1/2}\right] \qquad (1)$$

where N is the number of atoms in the metal. The parameter r_0 is the nearest-neighbour distance at 0 K and is introduced to normalize the distances. r_{ij} is the distance between the atoms i and j. ξ, q, A, p are parameters of the potential. The summation over j can be extended over several coordination shells ($r_{ij} < r_c$, cut-off radius). The exponential functions are truncated at a distance r_t and we interpolate both terms in relation (1) between r_t and r_c with a fifth-degree polynomial. This ensures continuity of the energy (at r_t and r_c) up to the second derivative and allows us to avoid discontinuities of the second-order elastic constants. Note that this polynomial is the only difference with respect to the classical tight-binding potential used in [14].

The four parameters ξ, q, A, p are adjusted according to the numerical values of the lattice parameters, the cohesion energy E_{coh}, the bulk modulus B and, for Au potential, the shear elastic constant $C' = (C_{11} - C_{12})/2$ (see table 1).

For Ni, the direct adjustment converges to unrealistic values of the four parameters. However an exact fit is unnecessary and we can fix one of the parameters. We choose to fix the parameter q as in [3] using a value often found in the literature of 2.7 [14]. When the value of q decreases, the adjustment becomes better and Cleri and Rosato [26] have taken the value 1.189 for q. We have chosen $q = 2.5$, because for a smaller value, the surface relaxation is a dilatation instead of a compression observed experimentally.

Furthermore, the energy difference between the fcc and the hcp crystals depends on the cut-off radius r_c. We choose the value of r_c to stabilize the fcc crystal and to get the

Table 1. The four experimental quantities to be fitted: r_0 (Å), E_{coh} (eV), B and $C'(10^{11}$ Pa) at $T = 0$ K.

	r_0 [50][a]	E_{coh} [51]	B [52]	C' [52]
Au	2.874	3.78	1.805	0.158
Ni	2.486	4.44	1.876	0.552

[a] With the thermal expansion, we have calculated the value of r_0 at 0 K.

greatest difference between these energies. Finally, the value of r_t is fixed so that the second derivative of the interpolation function has the fastest decrease possible. This criterion is important in order to avoid any instability in the determination of elastic constants. Table 2 gives the values of the adjusted parameters.

Table 2. Values of the potential parameters for the repulsive and attractive terms of the interatomic potential. A and ξ are in eV, p and q are dimensionless and the length r_t and r_c are normalized by the first-neighbour distance r_0 given in table 1.

		A	p	r_t/r_0	r_c/r_0
Repulsive term					
	AuAu	0.2227	10.3652	1.6585	1.980
	NiNi	0.1463	9.4996	1.6686	2.020
	AuNi	0.1805	9.9324	1.6250	1.964
		ξ	q	r_t/r_0	r_c/r_0
Attractive term					
	AuAu	1.8522	4.2873	1.5907	1.980
	NiNi	1.7117	2.5	1.3498	2.020
	AuNi	1.7806	3.3937	1.4703	1.964

To predict heteroatomic interactions from the homoatomic interactions, a classical procedure [27, 28] is to average the equivalent parameters to obtain the values of the corresponding unlike atom parameters. This gives a heteroatomic concentration-independent potential. This simple method is applied in this paper and has been validated on the Au–Ni solid solution [3]. We set $r_0^{AuNi} = (r_0^{AuAu} + r_0^{NiNi})/2$ and use an arithmetic average of p and q and a geometric average of A and ξ (see table 2).

2.2. *Static properties*

2.2.1. Structural properties The calculated elastic constants and vacancy formation energy are listed in table 3. These values are compared with experimental results extrapolated at 0 K [29] and calculations of the embedded atom method (EAM) [30, 31]. Moreover, the calculated deviation of Vegart's law for the solid solution is in good agreement with the experimental one. Our potential is very similar to the one used by Eymery *et al* [32, 3]. The main modification is the energy difference between the fcc and hcp phases. The calculated intrinsic stacking fault energies are compared with the experimental results [33] in table 4. Our results are too low, specially for Au, because the second-moment approximation of the electron density of states suffers intrinsic limitations that makes it unsuitable to describe the relative stability of the face-centred, hexagonal, and body-centred structures along the transition series [34].

Table 3. Calculated pure metal properties of Au and Ni. Elastic constants at 0 K are in 10^{11} Pa and the vacancy formation energy in eV.

	Au	Ni
C_{11}	2.016[a]	2.612[a]
	2.016[b]	2.273[b]
	2.023[c]	2.266[c]
C_{12}	1.700[a]	1.508[a]
	1.700[b]	1.677[b]
	1.703[c]	1.680[c]
C_{44}	0.454[a]	1.317[a]
	0.414[b]	0.918[b]
	0.381[c]	1.842[c]
E_v^f	0.94[a]	1.70[a]
	0.58[b]	1.35[b]
	0.55[c]	1.37[c]
	1.03[d]	1.63[d]

[a] Experimental [52, 54].
[b] This work.
[c] Eymery *et al* [32, 3].
[d] EAM [31].

Table 4. Intrinsic stacking fault energy γ_I in units of mJ m^{-2}.

	Au	Ni
γ_I	32[a]	125[a]
	1.5[b]	25[b]
	52[c]	

[a] Experimental [33].
[b] This work.
[c] LMTO calculation [53].

The surface energies obtained for the low-index faces, (100), (110), and (111), of both metals are presented in table 5. The surface energies are calculated by comparing the energy of a periodic slab of atoms to the energy of the same number of atoms in the bulk material. For both cases, the close-packed (111) face has the lowest surface energy, followed by the (100) and (110) faces. This table also contains the estimates, due to Tyson and Miller [29], of the surface energy based on liquid metal surface energies. We note that the calculated values are consistently smaller than these experimental values. Similar deviations have been obtained with the EAM [31].

2.2.2. *Phonon dispersion curves.* Phonon dispersion curves were obtained by expressing the model force constants in the quasiharmonic approximation [35]. The dispersion curves for Au and for Ni crystals are shown in figures 1 and 2, respectively, together with experimental results [36, 37]. These are in good agreement with experimental curves, especially near the border of the Brillouin zone, which is an excellent test for the interatomic potentials.

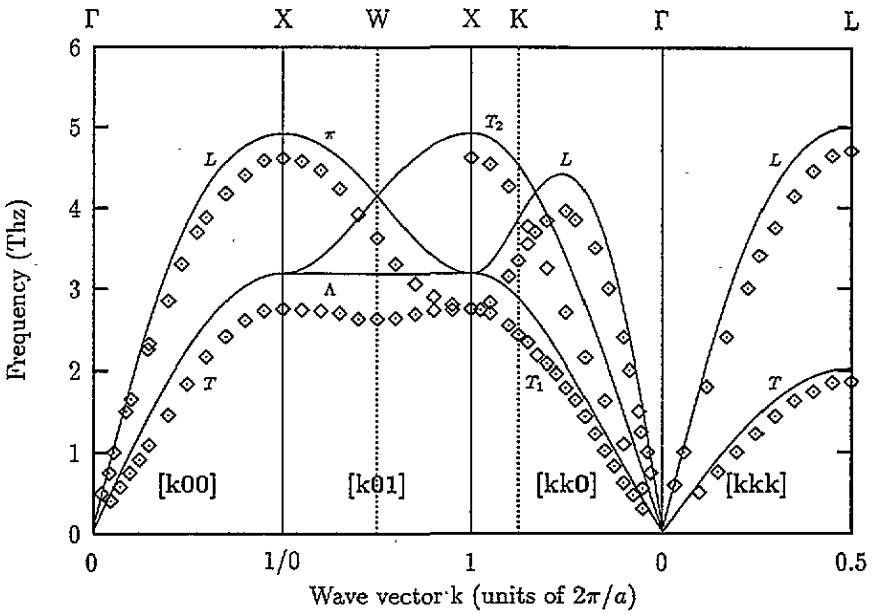

Figure 1. Phonon dispersion curves for fcc Au along the higher-symmetry directions. The experimental points (shown as square markers) are from Lynn *et al* [36]. The labels follow the convention of [37].

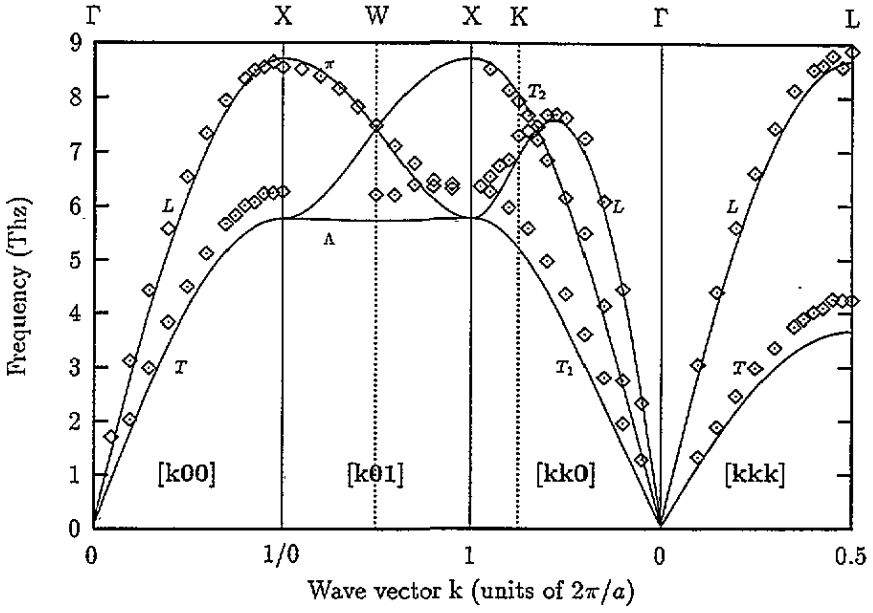

Figure 2. Phonon dispersion curves for fcc Ni along the higher-symmetry directions. The experimental data (shown as square markers) are from Birgeneau *et al* [37]. The labels follow the convention of [37].

2.3. Dynamical properties

All the following calculations of thermodynamic properties of metals at finite temperature were obtained by molecular dynamics (MD) simulations in the *NPT* isoenthalpic–isobaric

system, with the Gaussian technique [38]. The equations of motion for systems of 864 particles (corresponding to 6×6×6 basic cells) are integrated using a fifth-order Gear predictor–corrector algorithm [39, 40] with a variable time step, and imposing usual periodic boundary conditions. The variable time step is on average about 0.7 fs. The results obtained for various thermal properties of both metals are reported in table 6.

For Au, the melting point is usually considerably underestimated by the tight-binding potential [26, 32]. This low melting point is probably a result of too strong an anharmonicity of the potential: the calculated linear expansion coefficient α_{Au} is almost twice as big as the experimental one at room temperature and varies strongly at high temperature. So the lattice dilatation is too large and gives a melting point which is too low.

Table 5. Calculated surface energies of the low-index planes and the experimental average surface energy from Tyson and Miller [29] in units of mJ m^{-2}.

	Au	Ni
Experimental (average face)	1500	2380
(111)	430[a]	1380[a]
	388[b]	1275[b]
	790[c]	1450[c]
(100)	510[a]	1500[a]
	467[b]	1396[b]
	918[c]	1580[c]
(110)	535[a]	1640[a]
	980[b]	1730[b]

[a] This work.
[b] [32].
[c] EAM [31].

3. Au(001)/Ni multilayers

With this interatomic potential, a Au(001)/Ni multilayer structure has been studied as a function of the number of Ni monolayers and we have compared experimental results obtained by RHEED, HREM and EXAFS with our simulations.

In this study we assume that the Au/Ni interface are abrupt: this simplification permits us to take the competition between the Au/Ni interface energy and the volume energy of Ni strained film E_{vol}^{Ni} into account. Our study also concerns only the thin Ni layers before the appearance of defects like twins or dislocations. We restrict our study to the case of thick Au layers, i.e. with the bulk gold properties far from the interfaces.

Guided by experimental and numerical results we focus on six structures.

(i) *Pseudomorphic Ni[001]:* a pseudomorphic coherent [001] growth (i.e. Ni and Au have the same in-plane structure and parameters) of the tetragonal Ni which has been observed experimentally for a Ni thickness less than 5 monolayers.

(ii) *Bulk-like Ni[001]:* an incoherent [001] growth of Ni which has no extra volume energy, only an interface energy.

(iii) *Ni[011]:* a [011] growth of the fcc Ni which has been observed experimentally with a lot of stacking faults for a Ni thickness larger than 50 monolayers [24].

(iv) *Ni[111]:* an incoherent [111] growth of the fcc Ni. On the top of a Ag(001) substrate, numerical relaxations [10] have shown that Ni(111) is the most stable film at 0 K above 3.3 monolayers of Ni.

(v) *Ni(hcp):* a $[2\bar{1}\bar{1}0]$ growth of the hexagonal Ni because we will see that the tetragonal Ni can transform spontaneously into this hexagonal structure. The close-packed planes are perpendicular to the interfaces.

(vi) *Ni(4H):* a $[2\bar{1}\bar{1}0]$ growth of the Ni(4H) i.e. the stacking of close-packed planes (A, B and C types) with the periodic repetition of four planes ABAC. This structure is intermediate between the Ni(hcp) (repetition of the AB sequence) and the Ni(fcc) (repetition of the ABC sequence); it can be obtained from the Ni(fcc) with half the number of stacking faults as compared to Ni(hcp). The Au/Ni interface is coherent. Au(001) has a periodic stacking of an even number of atomic planes along the [100] direction as the Ni(4H) (and the Ni(hcp)) along the [0001] direction. X-ray diffraction results [24] support the occurrence of this structure.

The periodic simulation cell was taken to be an integer multiple of the substrate Au(001) square unit cell and as close as possible to an integer multiple of both the Ni(001) and Ni(111) surface unit cells. Optimal values were found to be 17 lattice units along the [100] direction and six lattice units along the [010] direction, resulting in 204 Au atoms/layer.

These sizes minimize any lateral strain if either a perfect Ni[111] or a pseudomorphic Ni[001] adlayer were to form. Additional simulations were performed with a 6×6 simulation cell which minimizes the strain induced in the bulklike Ni[001]. These lateral sizes have been kept constant during the minimization to take into account the stress resulting from the large thickness of Au layers in the real material studied.

On the other hand, the size of the periodic cell along the [001] growth direction has not been fixed but has been considered as a variable of the total potential energy and optimized, like the particle coordinates, during the numerical relaxation. Along the [001] direction, 20 or 21 Au monolayers were used (depending on the parity of the number of Ni monolayers, n, in order to respect the simulation cell periodicity). We have checked that this number is enough to get the bulk properties in the middle of the gold layer.

Figure 3 shows the formation energy per surface unit

$$E_f = \left(E_{total} - \mathcal{N}_{Au}E_{Au}^{Bulk} - \mathcal{N}_{Ni}E_{Ni}^{Bulk}\right)/S$$

versus the number of Ni atoms per surface unit $\nu_{Ni} = \mathcal{N}_{Ni}/S$. The variable ν_{Ni} allows us to compare structures with different atom numbers per layer.

From figure 3, we can distinguish two parts, below and above five Ni monolayers, which correspond to two different Ni states of minimal energy. This will be discussed in detail now.

3.1. Ni thickness less than five monolayers

3.1.1. Stability of the Ni pseudomorphic structure. The pseudomorphic Ni[001] structure on Au(001) is in tension in the plane of the growth, and this stress involves a tetragonal distortion of the Ni cell. Thus the pseudomorphic Ni[001] is a body-centred tetragonal (bct) Ni, the more stable structure corresponding in fact to almost the bcc structure. Ni(hcp), Ni(4H) and fcc Ni[011] are not stable and transform into the Ni(bct). The two last structures Ni[111] and bulklike Ni[001] remain unchanged. Their formation energies are above that of the pseudomorphic one because their incoherent Au/Ni interfaces have a high energy cost.

3.1.2. Comparisons with experiments. In figure 4, we show the distortion $d_{(002)} - d_{Au(002)}$ for Au/Ni multilayers with four Ni monolayers. We compare this result with those obtained by HREM [23] and by x-ray diffraction [24].

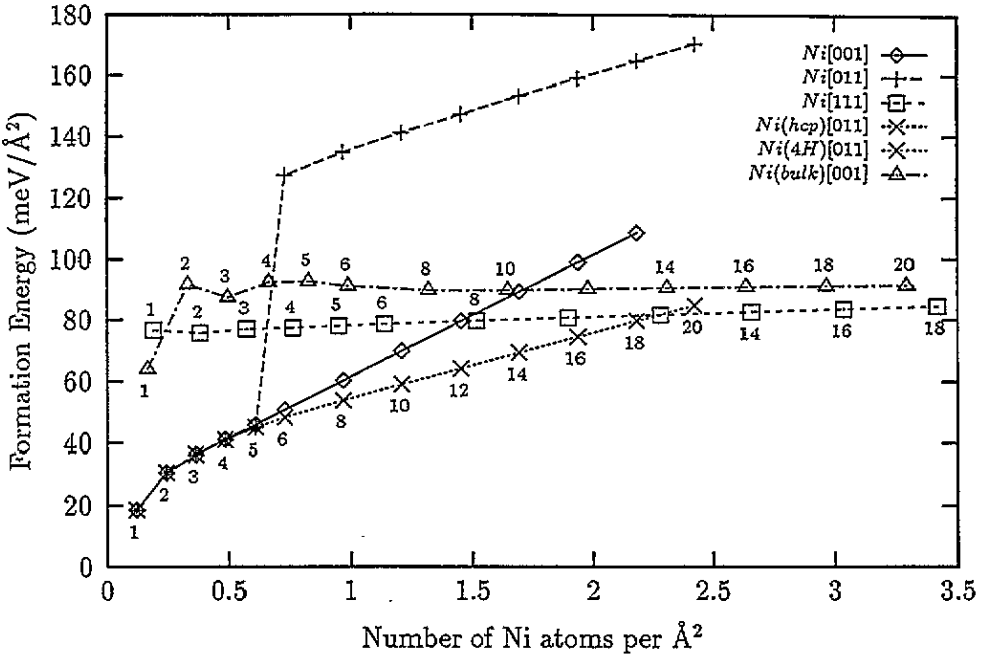

Figure 3. Formation energies of Au/Ni multilayers for different structures versus the number of Ni atoms per surface units. The numbers indicate the number of Ni monolayers.

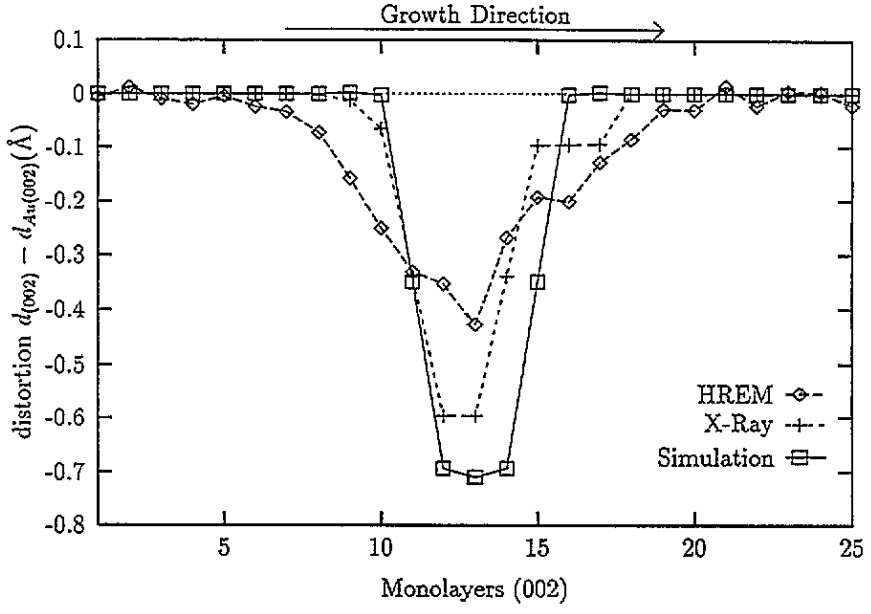

Figure 4. Distortion profile of the multilayer for four monolayers obtained along the (100) direction. The solid line is the calculated profile: the interfaces are abrupt and symmetrical. The diamonds and the crosses are respectively the experimental HREM [23] and x-ray [24] profiles which are asymmetrical and extend over a distance larger than the nominal number of Ni monolayers.

In [23] the authors measured, from an HREM image, the local distortion of the lattice along the direction perpendicular to the plane of the multilayer, using a image processing package. This method was first described by Bierwolf *et al* [41]. The main features of this analysis are the following:

(i) the lattice distortion is extended over distances larger than the nominal width of the Ni layers,

(ii) the profile is asymmetrical with respect to the growth direction; the Au/Ni interface being more abrupt than the Ni/Au interface.

The conclusion of the paper [23] was that these features were indicative of an intermixing of Au and Ni atoms at the interfaces.

The profile obtained by x-ray diffraction has the same features as that obtained by HREM but with much sharper interfaces i.e. the lattice distortion extends further than the Ni layers and the profile is asymmetrical.

This intermixing is not taken into account in the present simulation and thus the calculated profile is more abrupt but there is good agreement between the calculated curve and that obtained by x-ray diffraction. We will return to the concentration profile after a description of the exchange mechanism.

3.2. Ni thickness larger than five monolayers

3.2.1. Stability of Ni hexagonal structures. Above five monolayers, the tetragonal configurations are saddle points of the potential energy: they turn to a mixture of 4H and hcp when the tetragonal configuration is broken by a small perturbation. It appears from these simulations that the tetragonally deformed Ni undergoes a martensitic-like transformation resulting in a stacking of hexagonal planes perpendicular to the $(002)_{Au}$ planes (see figure 5). This results in two variants whose c axis is parallel to either $[100]_{Au}$ or $[010]_{Au}$. The orientation of the first one is Ni[0 0 0 1] along Au[1 0 0], Ni[0 $\bar{1}$ 1 0] along Au[0 1 0], and Ni[2 $\bar{1}$ $\bar{1}$ 0] along Au[0 0 1].

Ni(4H) and Ni(hcp) which are coherent with a Au(001) substrate are distorted. The distance between the close-packed planes which are aligned with the Au(200) planes is only 0.2% greater than in bulk fcc Ni. On the other hand, these close-packed planes are strained 6% in compression along [0 $\bar{1}$ 1 0] direction and the lateral shift between A-type and B-type planes is less than that found in an ideal hexagonal phase (see figure 5). Thus, above five monolayers, Ni is in compression, while below 5 monolayers, Ni is in tension.

Ni(4H) and Ni(hcp) structures have nearly the same formation energies, the two curves are indistinguishable in figure 3. The Au/Ni interface energies are identical: by reason of parity, Ni(4H) and Ni(hcp) are coherent with Au(001) unlike Ni[011]. The difference between 4H and hcp is the number of stacking faults: 4H has half as many stacking faults as hcp. Consequently Ni(4H) should have a lower energy than Ni(hcp). As our potential underestimates the stacking fault energy of the bulk Ni, our calculation could not predict which one is the most favourable.

From five to 16 monolayers, the three structures Ni[111], Ni[001] and Ni[011] have high formation energies due to the energy cost of incoherent interfaces. However, for 16 monolayers the curves of formation energies of Ni[111] and Ni[001] cross the curve of hexagonal Ni meaning that hexagonal Ni is less favourable than Ni[111] or Ni[001] which is contradictory with experimental results.

This discrepancy may come from the defects (twins, dislocations) which were not taken into account in the computations. Large simulation cells are necessary to simulate defects

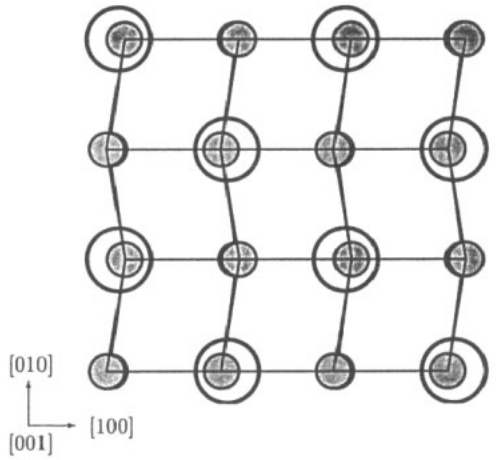

Figure 5. Perpendicular section to the direction of growth of a Au/Ni multilayer with 10 Ni monolayers. This is a distorted hexagonal phase with 6% compression along the [100] direction; the relative lateral shift between the A-type and the B-type close-packed planes is also smaller than that of an ideal hexagonal structure.

like twins and the competition between interface energy and volume energy of the Ni film which depends sensitively on stacking fault energy for these large thicknesses.

3.2.2. Comparisons with experiments. Results of these numerical relaxations are shown in figure 6 and compared to the HREM cross-section view [25]. Simulations of HREM images [42] have shown that in the case of an hcp structure (AB stacking), the holes are imaged as white spots. These holes correspond to the C empty sites. On the other hand, in the case of 4H (ABAC stacking) the atoms in the A close-packed planes in excess are imaged. Therefore, HREM plane views [42] of 25 Ni layers showed that the 4H stacking is in the majority.

For very large thickness (about 100 Å, i.e. 50 Ni monolayers) x-ray diffraction experiments show the occurrence of the Ni[011] fcc structure with stacking faults.

4. Ni film

4.1. Structure of Ni films

A transformation of the structure of the deposited Ni film has been observed by RHEED during the growth. Thus the study of the structure of Ni films on Au(001) substrate (transitory state during the growth) is as important as Au(001)/Ni multilayers which are the final states.

We have studied Ni films made of n monolayers in the range one to 24 on Au substrate of 20 monolayers (see figure 7). The Ni structure is tetragonal up to 2 monolayers. The hexagonal structure appears above three monolayers which is less than in the multilayer case (five monolayers). This is related to the fact that there is only one Au/Ni interface.

However we have found that the Ni(111) film has the lowest energy which is in disagreement with the experimental results [43, 13], but in agreement with the simulation

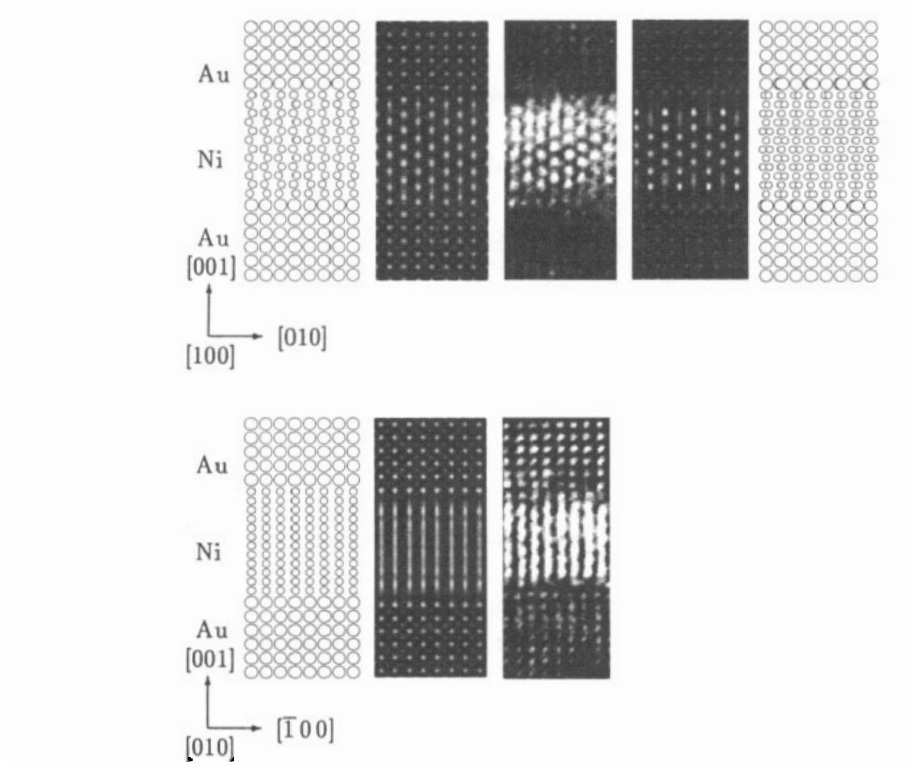

Figure 6. Calculated and experimental configurations made of 12 Ni monolayers between Au layers. Two different orientations are shown; top: cross-section perpendicular to the *c* axis of Ni(hcp) (left) and Ni(4H) (right); bottom: cross-section along the *c* axis. For each orientation we show the calculated configuration, simulated image and the experimental observation [23]. The white spots correspond to the C empty sites in the case of hcp or to the A sites in excess in the case of 4H.

result obtained by Bolding and Carter [10] in a similar system (Ag/Ni). Using the EAM potential, they found that a Ni(111) structure is the most stable film at 0 K for more than 3.3 monolayers, while experimental results show that Ni has a (001) growth on Ag [44].

This discrepancy with the experimental results can be explained if we take into account the covering of the Ni surface by a Au monolayer which drastically decreases the formation energies. Ni has a surface energy four times as high as that of Au and thus the system prefers to have a Au monolayer rather than a Ni monolayer on the surface. In this more realistic case our calculations show that the pseudomorphic Ni(hcp)[011] has the lowest formation energy (see figure 8). When a Au monolayer covers the Ni film, there are two Au/Ni interfaces. This is a penalty for the Ni(111) whose incoherent interface with Au(100) has a highest energy.

This phenomenon is similar to surface segregation which has been studied by Ducastelle *et al* [45] with a mean-field model using the tight-binding Hamiltonian. They found with Pt–Ni and Cu–Ag alloys that a surface sandwich with a pure element on top can exist. In table 7, we give the energy of formation versus the number of Au monolayers which cover the Ni film. We find that two Au monolayers covering the Ni film corresponds to the lowest energy.

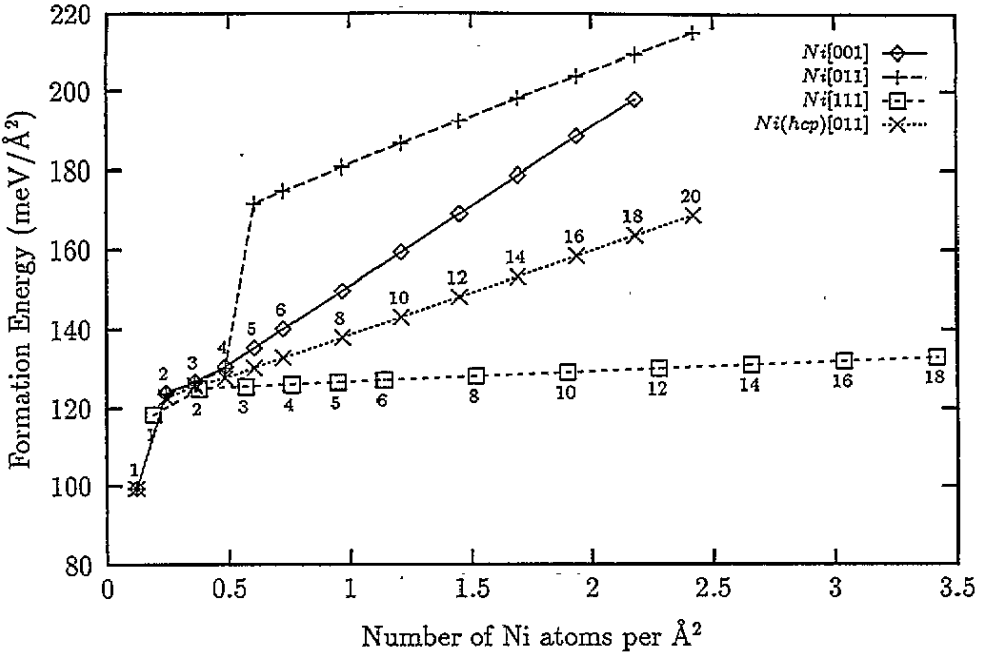

Figure 7. Formation energies of Ni films on a Au substrate for different structures versus the number of Ni atoms per surface unit. The numbers indicate the number of Ni monolayers.

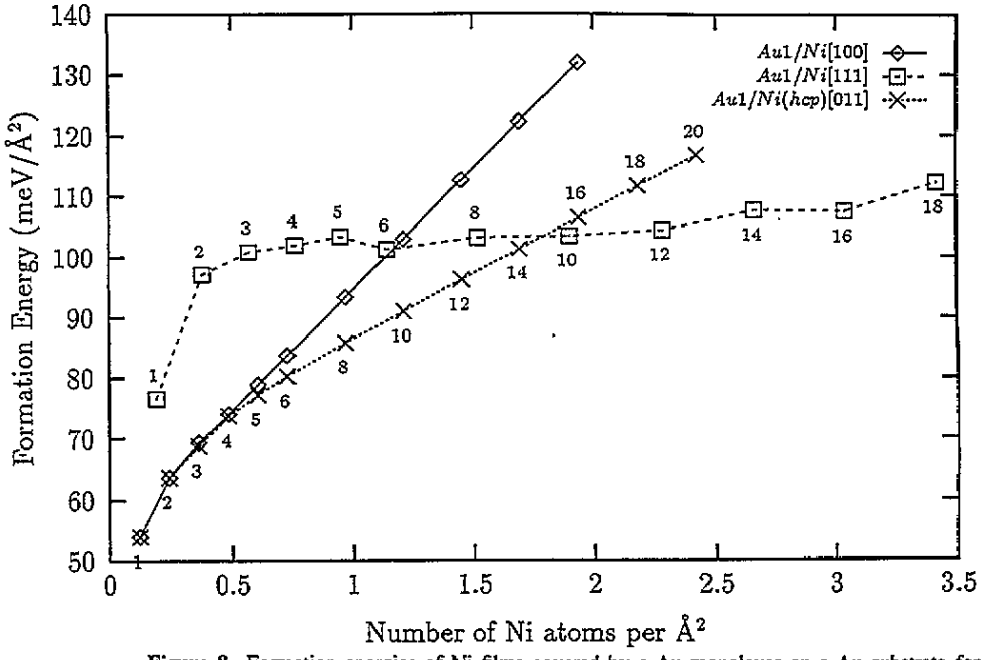

Figure 8. Formation energies of Ni films covered by a Au monolayer on a Au substrate for different structures versus the number of Ni atoms per surface unit. The numbers indicate the number of Ni monolayers.

4.2. Exchange mechanism

If Au atoms flow on the top layer, a spontaneous exchange mechanism between a Ni adatom and a Au atom of the top layer on surface (100) should exist. We do have observed this by

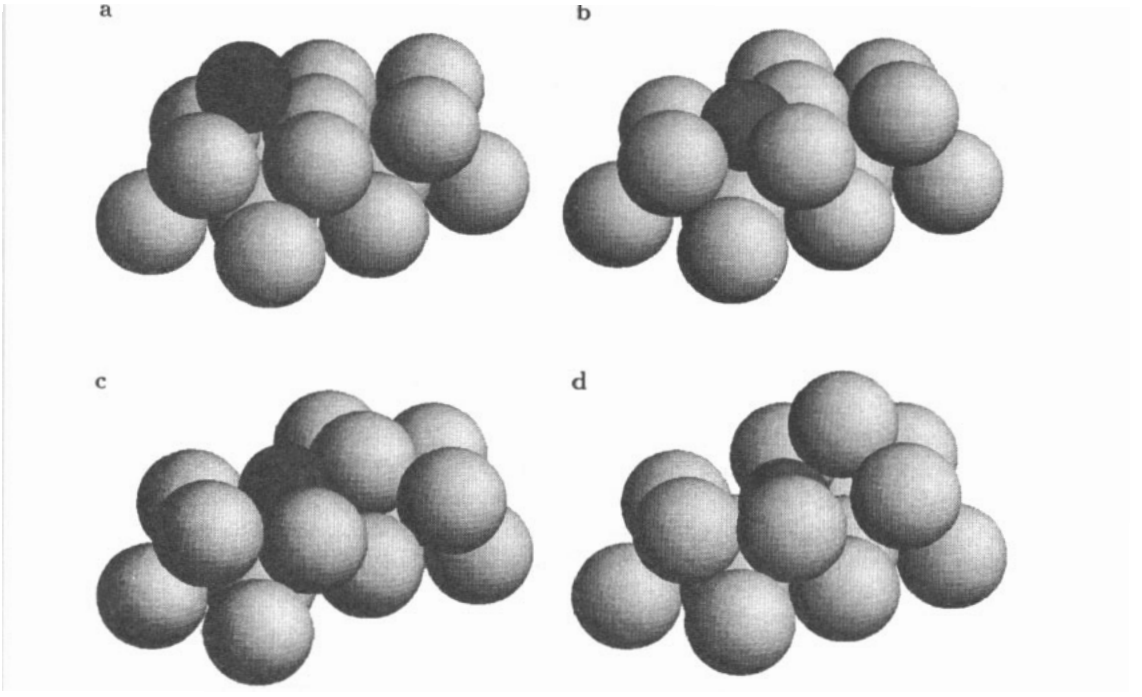

Figure 9. Four views of the exchange mechanism on the (100) surface between a Ni adatom and a Au atom on the top layer. (a) The Ni adatom stays on the Au surface. (b) It enters the top layer while the nearest atoms move away. (c) The Au atom is ejected from the top layer and (d) its initial position is now occupied by the Ni atom.

Table 6. Miscellaneous finite-temperature properties for Au and Ni calculated with the potential of the present work: melting temperature T_m (K), latent heat of fusion ΔH_m (kJ mol^{-1}), latent volume of fusion ΔV_m (%) and linear expansion coefficient α (10^{-5} K^{-1}) between 0 and 600 K. Experimental data in brackets are taken from Brandes [55].

	Au		Ni	
T_m	885	(1336)	1450	(1728)
ΔH_m	8.78	(12.8)	13.53	(17.2)
ΔV_m	6.9	(5.1–5.5)	5.5	(4.5–6.3)
α	2.43	(1.41)	1.55	(1.33)

molecular dynamics at different temperatures.

Figure 9 shows the different steps of the exchange mechanism at room temperature. This atomic exchange occurs in two steps. First the Ni adatom on the Au surface (view a) enters into the first surface layer (view b) when the two adjacent [110] rows have been moved away. Then the Au atom is ejected from the top layer (view c) and it becomes an adatom on the surface.

This diffusion mechanism has been investigated for Ni/Ni(100)[46], Cu/Cu(100) [47] and on Pt(001) [48]. Furthermore, this phenomenon has been taken as evidence for Ir adatoms on the Ir(001) surface by means of field ion microscopy (FIM) [49].

Thus this will help us to explain the growth of Au(001)/Ni multilayers and the chemical

Table 7. Formation energies (in meV) of a Ni monolayer (ML) and two Ni monolayers covered by Au monolayers versus the number of Au monolayers. Two Au monolayers which cover the Ni film correspond to the lowest formation energy.

Number of Au ML	1 Ni ML	2 Ni ML
0	131.07	155.51
1	85.66	95.42
2	81.16	93.63
3	82.18	94.20
4	81.99	94.09
5	82.02	94.11

profile observed experimentally (figure 4). When a Ni atom arrives on the Au(001) surface, it enters the top Au layer. Then, during the growth of the Ni film, Au atoms float on the surface and some are randomly trapped in the Ni film. This results in a slightly abrupt interface whose abruptness depends on the kinetic growth. When the deposited atoms are switched to Au, these atoms do not exchange with Ni atoms of the film, because of the lowest Au surface energy and they fill the uncompleted Ni planes. As the number of uncompleted Ni monolayers is large, the second interface is broader than the first one.

5. Conclusion

We have shown that during the growth the Ni films must be covered by Au atoms. This is explained as a result of energy considerations and we have described the exchange mechanism of the initial step of the covering. A martensitic transformation above five monolayers in the Ni layers results in the hexagonal structures (pure hcp or 4H). Our results are in good agreement with RHEED *in situ* observation [13], HREM [23] and x-ray diffraction measurements [24]. Better agreement between the measured and calculated values of the chemical profiles could be obtained by considering the possible mixing of the Ni and Au atoms in the layers close to the interface.

Acknowledgments

The authors wish to thank B Gilles for the experimental results and L Billard and A Marty for fruitful discussions. We also express our gratitude to F Willaime for providing us with the phonon codes.

References

[1] Luedtke W D and Landman U 1991 *Phys. Rev.* B **44** 5970
[2] Chaudhuri J, Gondhalekar V and Jankowski A F 1992 *J. Appl. Phys.* **71** 3816
[3] Eymery J, Lançon F and Billard L 1993 *J. Physique* I **3** 787
[4] Nandedkar A S 1993 *Acta Metall. Mater.* **41** 3455
[5] Nielsen L P, Besenbacher F, Stensgaard I, Lægsgaard E, Engdahl C, Stoltze P, Jacobsen K W and Nørskov J K 1993 *Phys. Rev. Lett.* **71** 754
[6] Lee C H, He H, Lamelas F, Vavra W, Uher C and Clarke R 1989 *Phys. Rev. Lett.* **62** 653
[7] Chamberod A, Dieny B, Eymery J, Gilles B, Hartmann J, Marty A and Redon O 1992 *J. Physique Coll.* IV **C3** 245
[8] Wu L, Shintaku K, Shinjo T and Nakayama N 1993 *J. Phys.: Condens. Matter* **5** 6515
[9] Brizard C, Pizzini S and Regnard J R 1994 *Solid State Commun.* **90** 147

[10] Bolding B C and Carter E A 1992 *Surf. Sci.* **268** 142
[11] Gao Y and Merkle K L 1990 *J. Mater. Res.* **5** 1995
[12] Gumbsch P, Daw M S, Foiles S M and Fischmeister H F 1991 *Phys. Rev.* B **43** 13 833
[13] Gilles B, Marty A, Patrat G, Vassent J I, Joud J C and Chamberod A 1994 *Mechanisms of Thin Film Evolution; Mater. Res. Soc. Symp. Proc.* vol 317, ed S M Yalisove, C V Thompson and D J Eaglesham (Pittsburg, PA: Materials Research Society)
[14] Rosato V, Guillopé M and Legrand B 1989 *Phil. Mag.* A **59** 321
[15] Ducastelle F 1970 *J. Physique* **31** 1055
[16] Ducastelle F 1991 *Computer Simulation in Materials Science: Interatomic Potentials, Simulation Techniques and Applications (NATO Advanced Study Institute Series)* ed M Meyer and V Pontikis (Dordrecht: Kluwer) pp 233–53
[17] Willaime F and Massobrio C 1989 *Phys. Rev. Lett.* **63** 2244
[18] Guillopé M and Legrand B 1989 *Surf. Sci.* **215** 577
[19] Allan G and Lannoo M 1973 *Surf. Sci.* **40** 375
[20] Allan G and Lannoo M 1988 *Phys. Rev.* B **37** 2678
[21] Loisel B, Gorse D and Pontikis V 1989 *Surf. Sci.* **221** 365
[22] Rosato V, Cardellini F and Cleri F 1993 *Phil. Mag.* B **68** 845
[23] Bayle P, Deutsch T, Gilles B, Lançon F, Marty A and Thibault J 1994 *Ultramicroscopy* **56** 94
[24] Gilles B, Brizard C, Bayle P and Marty A 1994 *Thin Films: Stresses and Mechanical Properties V; Mater. Res. Soc. Symp. Proc.* vol 356 (Pittsburg, PA: Material Research Society) at press
[25] Bayle P, Deutsch T, Gilles B, Lançon F, Marty A, Thibault J, Colliex C and Tence M 1994 *Defect–Interface Interactions; Mater. Res. Symp. Soc. Proc.* vol 319, ed E P Kvam, A H King, M J Mills, T D Sands and V Vitek (Pittsburg, PA: Material Research Society)
[26] Cleri F and Rosato V 1993 *Phys. Rev.* B **48** 22
[27] Rafii-Tabar H and Sutton A P 1991 *Phil. Mag. Lett.* **63** 217
[28] Ackland G J and Vitek V 1990 *Phys. Rev.* B **41** 10 324
[29] Tyson W R and Miller W A 1977 *Surf. Sci.* **62** 267
[30] Daw M S and Baskes M I 1984 *Phys. Rev.* B **29** 6443
[31] Foiles S M, Baskes M I and Daw M S 1986 *Phys. Rev.* B **33** 7983
[32] Eymery J 1992 *Thèse* L'Institut National Polytechnique de Grenoble
[33] Hirth J P and Lothe J 1982 *Theory of Dislocations* 2nd edn (New York: Wiley)
[34] Ducastelle F 1974 *J. Physique Coll.* C7 79
[35] Ashcroft N W and Mermin N D 1976 *Solid State Physics* (Tokyo: Holt-Saunders) ch 22
[36] Lynn J W, Smith H G and Nicklow R M 1973 *Phys. Rev.* B **8** 3493
[37] Birgeneau R J, Cordes J, Dolling G and Woods A D 1964 *Phys. Rev.* **136** 1359
[38] Hoover W G 1986 *Molecular Dynamics Lecture Notes in Physics* vol 258 (Berlin: Springer) pp 22
[39] Nordsieck A 1962 *Math. Comput.* **16** 22
[40] Lechevallier G and Moreau G-M *Projet de Fin d'Études* ENSIMAG
[41] Bierwolf R, Hohenstien M, Phillip F, Brandt O, Crook G E and Ploog K 1974 *J. Physique Coll. Suppl.* 12 **35** C7 p 67
[42] Bayle P 1994 *Thèse* Université Joseph Fourier
[43] Gilles B, Eymery J, Marty A, Joud J C and Chamberod A 1992 *Interface Dynamics and Growth; Mater. Res. Soc. Symp. Proc.* vol 237, ed K S Liang, M P Anderson, R F Bruinsma and G Scoles (Pittsburg, PA: Materials Research Society) p 511
[44] Bruce L A and Jaeger H 1977 *Phil. Mag.* **36** 1331
[45] Ducastelle F, Legrand B and Tréglia G 1990 *Prog. Theor. Phys. Suppl.* **101** 159
[46] Perkins L S and DePristo A E 1993 *Surf. Sci.* 294 67
[47] Black J E and Tian Z J 1993 *Phys. Rev. Lett.* **71** 2445
[48] Kellog G L and Feibelman P J 1990 *Phys. Rev. Lett.* **64** 3143
[49] Chen C and Tsong T T 1990 *Phys. Rev. Lett.* **64** 3147
[50] *Thermophysical Properties of Matter: Thermal Expansion (The TRPC data Series)*
[51] Kittel C 1972 *Introduction à la Physique de l'État Solide* 3rd edn (Paris: Dunod)
[52] Simmons G and Wang H 1971 *Single Crystal Elastic Constants and Calculated Aggregated Properties: a Handbook* 2nd edn (Cambridge, MA: MIT Press)
[53] Schweizer S, Elsässer C, Hummler K and Fähnle M 1992 *Phys. Rev.* B **46** 14 270
[54] Seeger A, Schumacher D, Schilling W and Diehl J 1970 *Vacancies and Interstitials in Metals* (Amsterdam: North-Holland)
[55] Brandes E A 1983 *Smithells Metals Reference Book* 6th edn (Washington, DC: Butterworth)